Dynamic fracture of CrN coating by highly-resolved nano-impact

Xiangru Shi[a,1], Heng Li[a,1], Ben D. Beake[b], Mingdong Bao[c], Tomasz W. Liskiewicz[d], Zhengming Sun[a], Jian Chen[a*]

a. School of Materials Science and Engineering, Jiangsu Key Laboratory for Advanced Metallic Materials, Southeast University, Nanjing 211189, China

b. Micro Materials Ltd., Willow House, Yale Business Village, Ellice Way, Wrexham, LL13 7YL, United Kingdom

c. School of Materials Science and Chemical Engineering, Ningbo University of Technology, Ningbo 315211, China

d. Institute of Functional Surface, School of Mechanical Engineering, University of Leeds, Leeds LS29JT, United Kingdom

[1] These two authors contribute equally.

* Corresponding author. Tel: +86 25 52090688. E-mail address: j.chen@seu.edu.cn (Jian Chen)

Abstract

Nano-impact testing has provided localized high strain rate deformation information in either (i) repetitive impact for fatigue of brittle materials or (ii) high-resolution data acquisition of single impacts for energy dissipation and dynamic hardness in ductile materials. The current study focusses on whether high-resolution data acquisition can be used to determine fracture occurring during a single impact event. A PVD CrN coating on 42CrMo4 high speed steel (HSS) was impacted with a cube corner indenter over a range of different acceleration forces. By analyzing the high precision depth-time curves during the first contact phase of the impact, an abrupt depth change was observed at and above 30 mN acceleration force. Focused ion beam technology confirmed through-thickness coating fracture without delamination on tests where the step was observed. The step was absent at lower force or on the more ductile HSS throughout the load range. The fracture dissipated energy and fracture toughness of the coating was estimated under 50 mN acceleration force based on the analysis of impact energy. The calculated dynamic fracture toughness of CrN coating is in the range of 2.75-7.74 MPa•$m^{1/2}$, depended on the indenter geometry constant, which is comparable with the reported value of about 3.13 MPa•$m^{1/2}$.

Keywords: CrN coating; nano-impact; failure mechanism; fracture toughness

1. Introduction

Due to their high hardness, good wear performance and corrosion resistance, transition metal nitride coatings such as chromium nitride (CrN) are widely used to protect and improve the lifetime of cutting tools for high-speed machining [1-3]. However, intrinsic brittleness accompanied by cracking under the harsh conditions of high stress and high strain rate is a significant concern as this can significantly degrade their performance [4.5]. Overcoming this limitation is a serious challenge when the cutting conditions involve repetitive contact, as in milling and interrupted turning [6-8].

Nano-impact tests are proving effective in the study of localized dynamic failure of thin hard coatings. The nano-impact test is a dynamic instrumented impact indentation with nanoscale depth resolution, which can probe the dynamic deformation and failure of various bulk materials and coating systems[9-13]. Repetitive nano-impact can simulate different coating damage scenarios including nano-fatigue, erosion, and wear[14-18]. In earlier studies Beake *et al.* [18.19] used the repetitive nano-impact testing to evaluate the fracture properties and fatigue wear of tetrahedral amorphous carbon coatings on silicon and CrAlTiN coating. Bouzakis *et al.*[5] investigated the brittleness of PVD TiAlN coatings with graded mechanical properties using repetitive nano-impact at various loads and 3D-FEM model, finding that the film failure initiation and evolution depended on the ratio of the film yield stress to rupture stress. Faisal *et al.*[16] employed a combination of repetitive nano-impact, multiple loading cycle nanoindentation tests and molecular dynamics simulations to provide information on the life and failure mechanism of diamond-like carbon coatings.

So far, most studies using the nano-impact method have focused on phenomenological analysis, for example, recording the time at which a sudden depth change in the displacement-time curves occurred. This type of behaviour is often correlated with cracking, and the probability of its occurrence after a given number of impacts is used to evaluate the resistance to fatigue failure [9.20]. However, there are limited studies quantifying this dynamic fracture. Recently, Frutos *et al.*[13] carried out repetitive

nano-impact with different impact energies to study the fracture toughness of α-Al_2O_3 using a cube-corner indenter. By assuming the crack geometry, the dynamic indentation fracture toughness was determined by the indentation model of Lawn and co-workers[21]. Although these studies show the potential of nano-impact in extracting detailed information on the fracture dynamics, the complex repetitive impact procedure makes the analysis difficult due to cracking phenomenon and resulting change in contact geometry, leading to decreased accuracy.

As an alternative to these repetitive impact tests, single nano-impact tests with a high data acquisition rate have been used to investigate the dynamic plastic deformation of elastoplastic materials [21]. Based on the one-dimensional contact model by Andrews *et al.* [22], Constantinides *et al.*[24] investigated the dynamic hardness for Al and Au using the dissipated energy approach. Abhi Ghosh *et al.* [23] studied the dynamic impact size effect and formation mechanism of Al and Ni by the change of energy during nano-impact process. It was found that the impact energy has a close relationship to plasticity. For brittle materials, Jennett *et al.*[17] suggested that the indentation fracture toughness could be determined by impact energy analysis. The authors demonstrated that the fracture events can be caught by the system and strongly depend on the impact energy and indenter geometry. Wheeler and Gunner [20] explored the impact fatigue of a sol-gel coating on stainless steel using high-speed acquisition and found that the evolution of dynamic hardness with continued impact could be used to identify the coating delamination. However, there are limited studies using single nano-impact to extract the dynamic fracture events. Furthermore, to the best knowledge of the authors, there are no reports analysing and quantifying the dynamic fracture for hard coatings using this method.

In this study, single nano-impact tests were carried out on a CrN coating at different impact energies using a blunt cube corner indenter. The dynamic contact was analyzed to extract the energy dissipation during the nano-impact process. By determining the cracks geometry by FIB-SEM, a fracture mechanism is proposed and dynamic

indentation fracture toughness estimated using dissipated energy and indentation fracture model.

2. Experimental Section

2.1. Materials and characterization

The CrN coating was deposited using cathodic arc evaporation in a commercial METAPLAS MZR-323 PVD reactor on 42CrMo4 high speed steel. The deposition was carried out at 450 ºC using a DC bias of 250 V in a high purity N_2 gas with a mass flow of 200 sccm. The deposition time was 60 min resulting in 2 μm of coating thickness. The substrate and the CrN samples were labeled as HSS and CrN/HSS in this study.

The surface morphology was determined using Leica DMI8C optical microscope. The surface roughness was measured by SURFTEST SJ-210 (Mitutoyo, Japan). XRD phase analysis was performed with a D8-Discover X-ray spectrometer (Bruker, Germany) from 20 to 90°, with the scanning rate of 3° min^{-1} at room temperature. The focus ion beam (FIB) facility was adopted to obtain the cross-sectional images of the impact craters, with further examination by scanning electron microscope (SEM) using working voltage of 20 kV.

2.2. Nanoindentation testing

Nanoindentation measurements were performed to set maximum depths with the NanoTest Vantage system (Micro Materials Ltd, UK) with a Berkovich indenter. The instrument was calibrated following the procedure outlined in ISO14577[25]. The maximum indentation depth was set at 100, 300, 400, 800 and 1200 nm, which correspond to those in the nano-impact tests. The loading and unloading rates for different maximum depths were set at 2-10 mN/s. The hold time at the peak force was 10 s and each test was repeated 10 times. The hardness (H) and reduced elastic modulus (E_r) were obtained by power-law fitting (Oliver and Pharr analysis) of unloading curves [26]. The reduced elastic modulus E_r is defined by Eq. (1).

$$\frac{1}{E_r} = \frac{1-v_i^2}{E_i} + \frac{1-v^2}{E} \quad (1)$$

in which E, v and E_i (1140), v_i (0.07) are the elastic modulus and Poisson's ratio of the sample and indenter, respectively.

2.3. Nano-impact testing

Nano-impact experiments were conducted using the "Dynamic Hardness" [single impact] option of the impact module of the NanoTest system with a cube corner indenter. To avoid the damage of the hard indenter during high-strain rate nano-impact testing, the indenter was well-worn through previous testing so that its geometry was that of a truncated cube corner indenter with end radius ~5 μm. The configuration utilized a solenoid fixed on the worktable and a ferromagnetic bead on the bottom of the pendulum (see ref [12] for more details of the setup). The solenoid connected to a timed relay can attract and hold the pendulum against a given accelerating force generated by the load cell. In this study, the accelerating forces (AF) were set at 10, 30, 50 mN, and five repeated tests were conducted at different positions for each load. The indenter was then positioned at a set accelerating distance (*AD*) of 15 μm from the sample. Once the solenoid was activated, the pendulum was released and accelerated towards the sample producing a ballistic trajectory of the pendulum. The instantaneous depth change as a function of time was recorded for each individual impact.

3. Results and Discussion

3.1 General characterization

The surface morphology and cross-sectional microstructure of the CrN coating are shown in Fig. 1(a). The surface morphology is typical for an arc deposited coating, with small particles of several microns diameter on the surface [27.28]. The R_a surface roughness of the CrN coating was (0.048 ± 0.006) μm. The cross-section (inset in fig. 1(a)) shows a dense and uniform columnar structure across the entire 2.0 μm thickness. XRD curves of the HSS substrate and the coating with indexed peaks are shown in Fig. 1(b), confirming that the CrN coating has preferred (111) orientation.

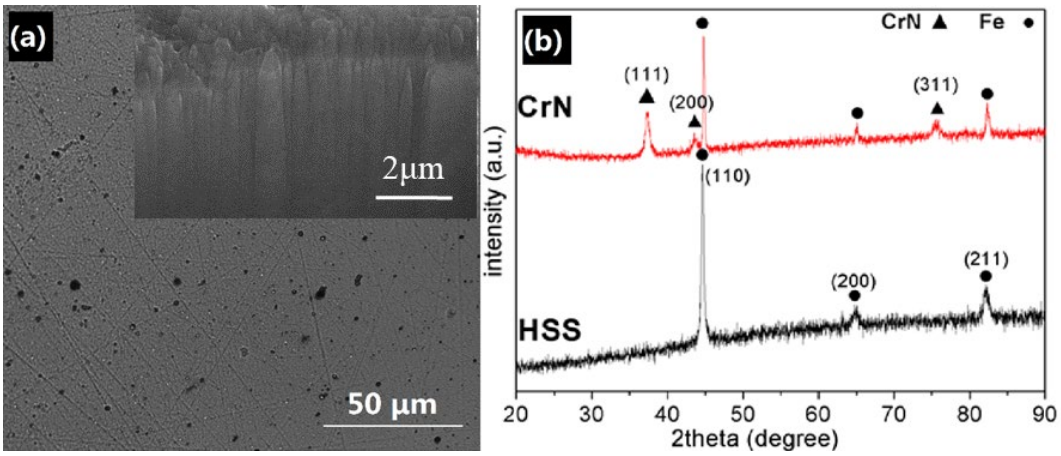

Fig. 1. (a) Surface morphology of CrN coating with the inset of cross-sectional image, (b) XRD phase diagram of the substrate and the CrN coating.

3.2 Nanoindentation

Fig. 2(a) shows typical force-displacement curves for HSS and CrN/HSS. For a given indentation depth, the applied load on CrN/HSS sample required is much larger indicating significantly higher indentation resistance for CrN coating. The intrinsic hardness (H) of the CrN coating is ~21 GPa at 100 nm contact depth, corresponding to ~5% of the coating thickness (Fig. 2(b)). At a relative indentation depth of 0.05 the entire plastic deformation zone should occur within the coating, and the effect of the elastic deformation of the substrate is almost negligible [29]. As the contact depth increased the composite mechanical response became increasingly dominated by the mechanical properties of HSS substrate, and H and E_r of CrN/HSS slowly approach that of the HSS (Fig. 2(b,c)). The strain to break parameter (H/E_r)[30.31] in Fig. 2(d) is inversely related to the plasticity index defined as the ratio of plastic work to total work for nanoindentation [32]. H/E_r exhibits similar trends with increasing depth as the H.

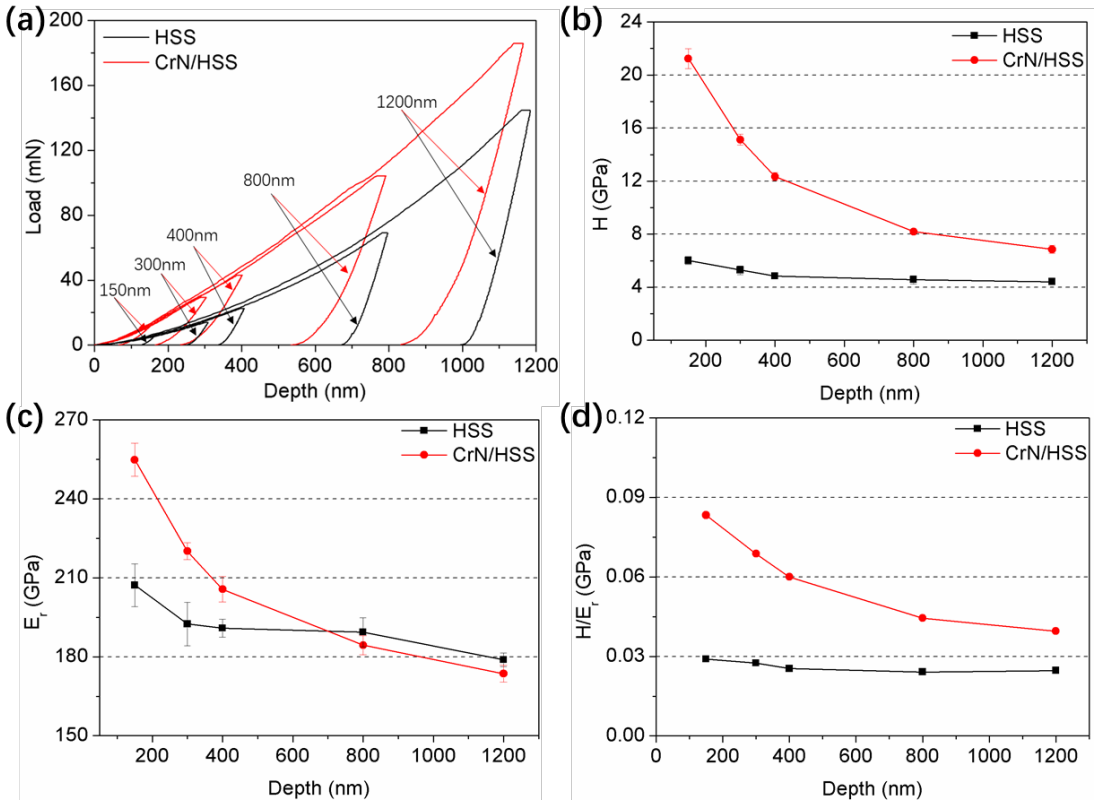

Fig. 2. (a) Typical nanoindentation curves for CrN/HSS and HSS at different indentation depths, and depth dependence of (b) hardness H, (c) elastic modulus E_r, (d) H/E_r ratio.

3.3 Nano-impact

3.3.1 Features in nano-impact time-depth curves

Using high data acquisition rate of dynamic impact testing setup, the impact depth h can be monitored continuously as a function of impact time t. As can be observed in Fig. 3a, the pendulum accelerates towards the surface of the sample from a given impact distance of 15 μm. After first impact cycle, the indenter bounces several times until it comes to rest. Comparing the maximum depth (h_m) after multiple cycles, it was found that h_m reached its maximum value at the first contact. Therefore, it was assumed that the plastic deformation of the material was completed after the first impact, and the subsequent impacts were dominated by elastic deformation. Recently Wheeler and his coworkers [33] also confirmed this assumption on a copper sample using a modified system with a catching solenoid to prevent rebounding impacts.

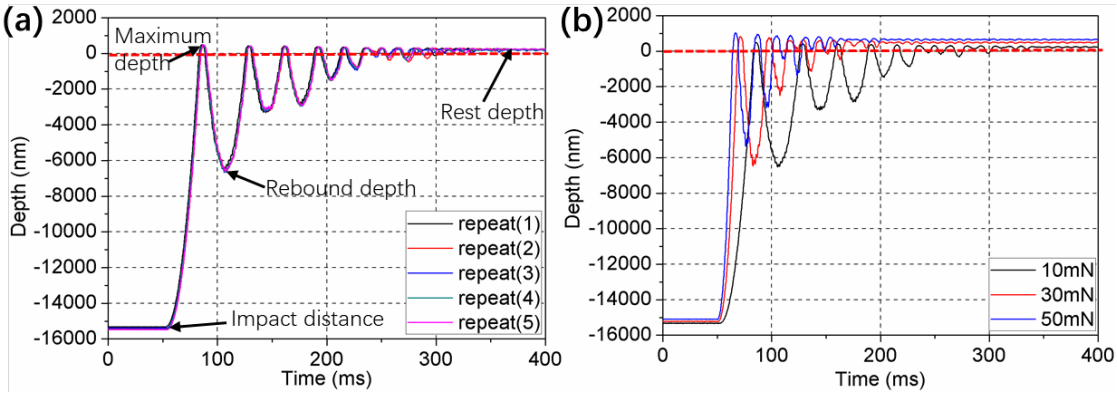

Fig. 3. Typical dynamic impact displacement-time (*t-h*) curves for CrN/HSS at (a) 10mN with five repeats, (b) different accelerating load from 10-50mN.

For CrN/HSS there is excellent reproducibility at 10 mN (fig. 3(a)) but at 30 and 50 mN there was more variability. More details were revealed by analyzing the impact curve with the derivative impact velocity (v)-time (t) during the first impact cycle as shown in Fig. 4. At a given acceleration force, the pendulum was accelerated towards the surface until the contact occurred, at which point the velocity of the indenter reached the peak value (v_0), and then the indenter was slowed down by the material resistance until reaching the maximum depth, h_m at $t = t_1$. During the indentation phase, the kinetic energy of the pendulum was converted to the revisable elastic work and/or irreversible plastic work. Afterwards, the stored elastic energy in the material was released resulting in acceleration of the indenter and rebound. It should be noted, the impact velocity decreased rapidly when the indenter contacted with the surface of the hard coating. This is a little different with our previous study by using a shaper Berkovich indenter to impact the soft materials of Al, Cu, Fe and Ti6Al4V, where the contact velocity changed slowly[34]. This phenomenon may be attributed to high hardness of CrN coating and larger contact area with blunt cube corner. Although the maximum impact velocity(v_0) and initial contact surface is a clearly identifiable signal in the curves, the identification of the rebound velocity v_2 when the indenter detach from the sample is less obvious. In this current study, the residual depth (h_r) at the end of the impact process was used to be as the detachment point and the rebound velocity was obtained.

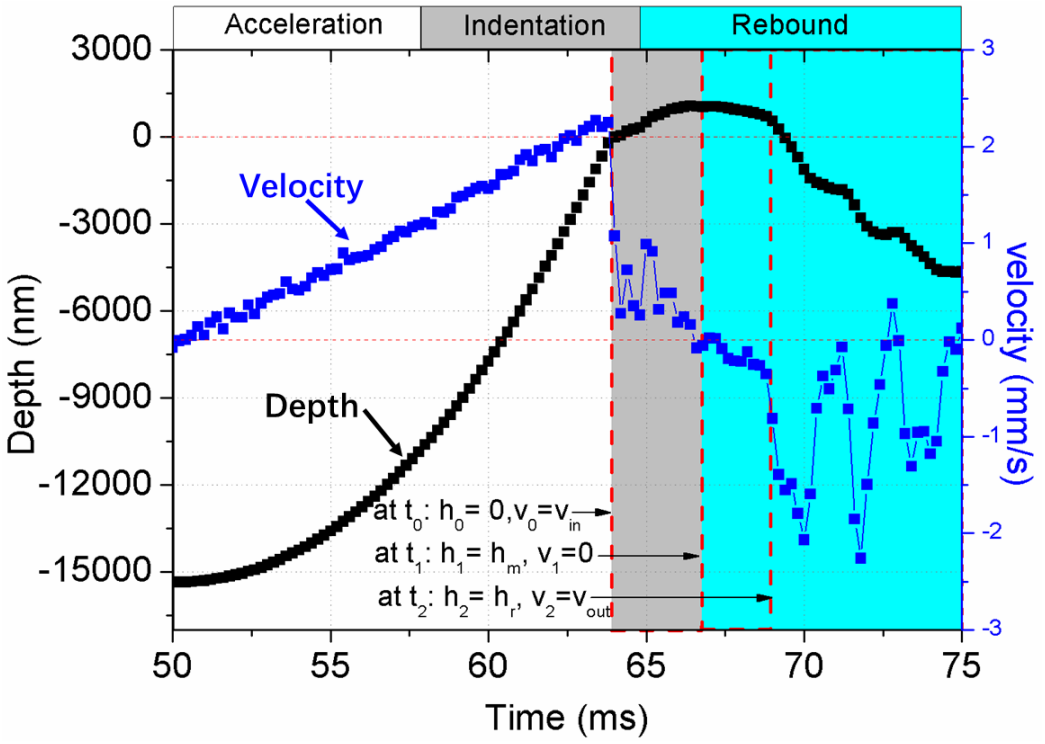

Fig. 4. Typical depth and velocity evolution as a function of time during the first impact cycle.

The average values of maximum depth (h_m), residual depth (h_r), impact and rebound velocity (v_{in} and v_{out}) during five repeated tests for HSS and CrN/HSS samples are shown in Fig. 5(a-f). The approximately constant v_{in} value and negligible error of the five repetitions for the pure substrate and coating at a given acceleration force indicate the very high repeatability. All of the data except v_{in} for CrN coating exhibit larger error bars than the substrate, which may be caused by the formation of some micro-cracks in the coating during the impact process. It has been shown recently[35] that the onset of variability in repetitive impact tests can provide a useful additional metric for the onset of cracking. At 10 mN there is very good consistency in h_m on CrN/HSS but at 30 mN there is greater test-to-test variability, suggetive of cracking in at least some of the tests at this load. The lower h_m of the CrN coating indicates an enhanced impact resistance and plastic deformation resistance than the HSS substrate.

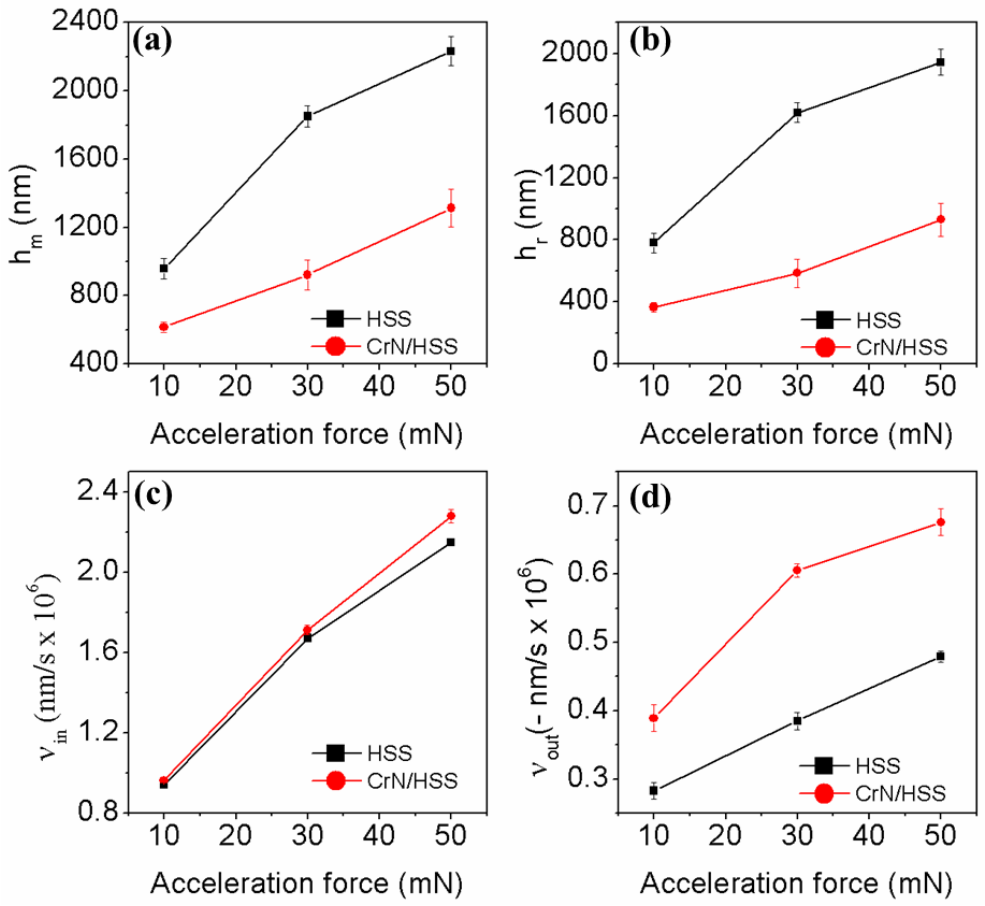

Fig. 5. Variation in the (a) maximum depth (h_m), (b) residual depth (h_r), (c) impact velocity (v_{in}), (d) rebound velocity (v_{out}).

Fig.6 shows the *t-h* curves of the HSS and the CrN/HSS during the first contact phase. It is interesting to notice that all the *t-h* curves for the HSS and that for CrN/HSS at 10mN show continuous smooth curves, while those for the CrN/HSS at higher *AF* (30 and 50 mN) exhibit a short irregular 'plateau' period during the indentation stage as indicated by the circle in Fig. 6b. A similar phenomenon has been reported widely in the multiple nano-impact testing for evaluating the fatigue resistance of thin films. Beake *et al.* [9]noted the presence of a short 'plateau' period where the depth remains virtually constant before a more rapid change in depth-time curves which corresponded to material removal of tetrahedral amorphous carbon films. Wheeler *et al.* [9] concluded that a single rapid increase in the penetration depth before an approximately stationary values observed in the repetitive impact curves is related to fracture and removal of the coating and penetration of the substrate, while a series of small jumps in penetration

depth reflected the cohesive failure with delamination fractures. However, the present study is the first time this phenomenon has been observed in the single nano-impact curves with high data acquisition rate during the indentation phase on the surface of hard coatings. To further verify the fracture and failure behaviors of CrN hard coatings, surface and cross-sectional morphology of the impact craters of the coating at different *AF* were investigated by SEM.

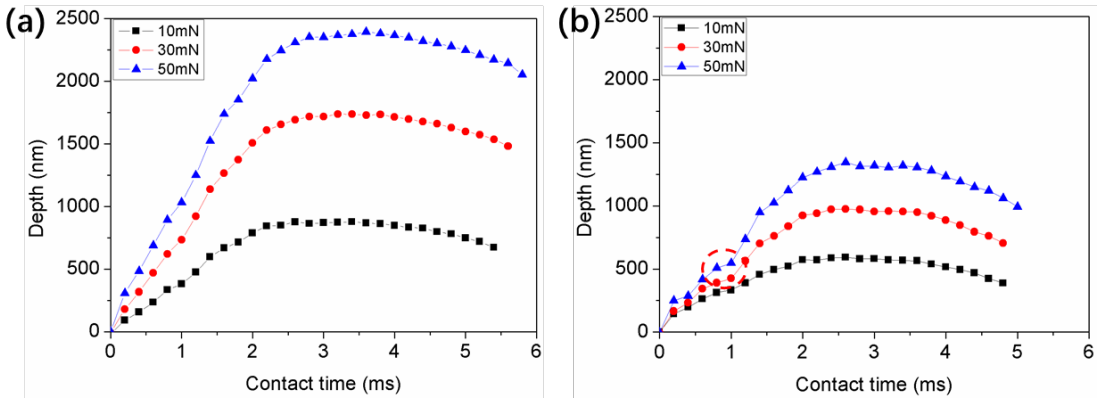

Fig. 6. The *t-h* curves during first contact cycle with different acceleration forces (a) HSS, (b) CrN/HSS (the circle highlights the sudden changes during indentation stage).

3.3.2 Typical fracture morphology and failure mechanism of CrN coating

As shown in Fig. 7 (a, b), the residual impression at 10 mN is faint and there is slightly irregular scar on the surface in agreement with the result in Fig. 6b. The irregular mark is caused by the blunt tip. On increasing the *AF* to 30 mN (Fig. 7 (c, d)), the residual impression becomes more obvious, where material removal and peripheral cracking can be clearly seen. At the highest *AF* of 50 mN, a large ring-like crack is formed. The images show that when impacted with the blunt tip the CrN coating is mainly plastically deformed at 10 mN, and undergoes cracking and material removal at 30 mN which becomes more pronounced at 50 mN. The above surface morphology results indicate that the real-time *h-t* data recorded during nano-impact can not only show the different contact phases but also provide information on cracking.

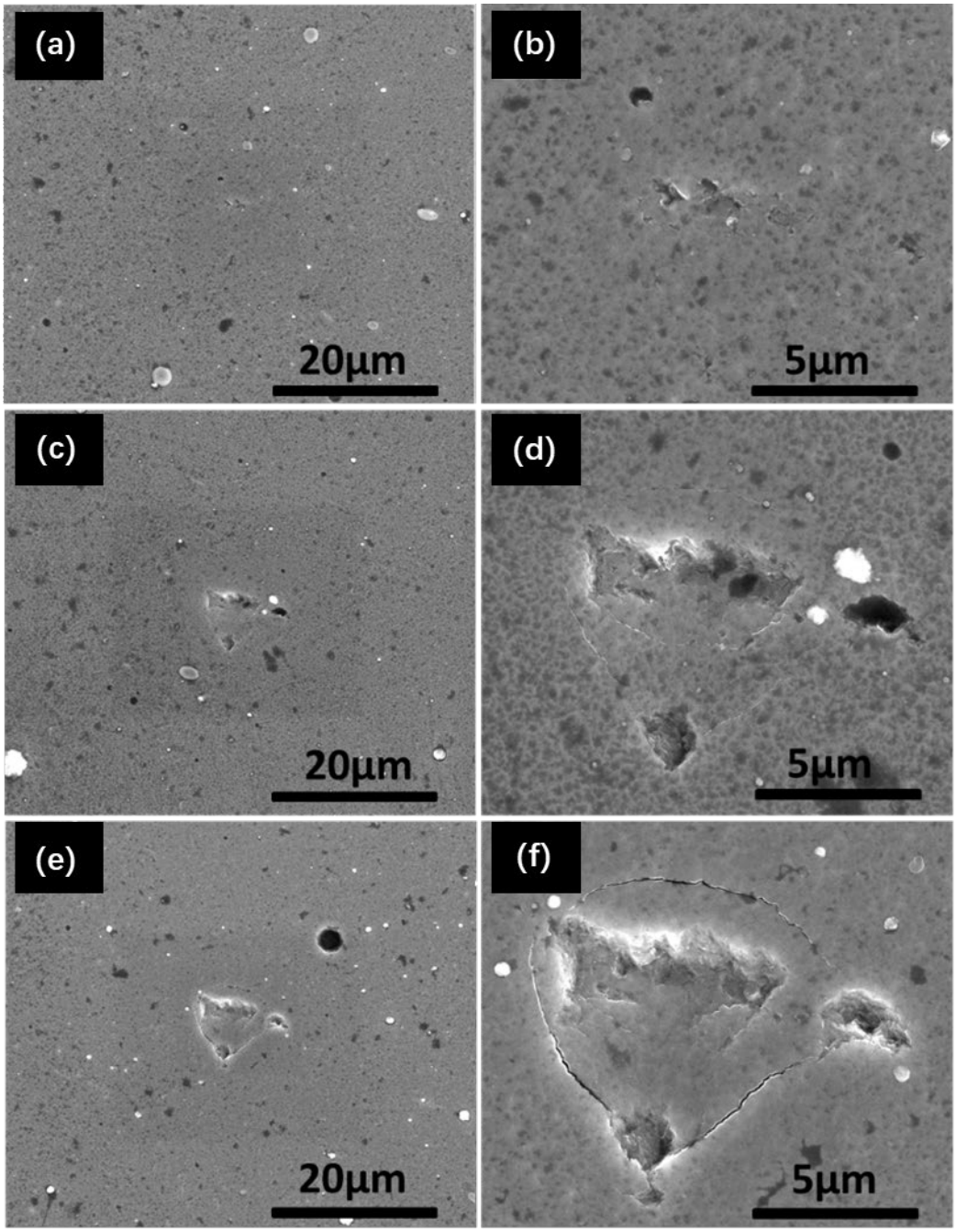

Fig. 7. Surface damage on CrN/HSS under different acceleration forces: (a, b) 10mN, (c, d) 30mN, (e, f) 50mN.

Surface morphological observation indicates that the ring-like cracking induced by nano-impact on CrN/HSS is dependent on the applied impact energy. However, from the top-view images information regarding the propagation of the cracks and the effects of interface and substrate is necessarily limited. To provide this information FIB-milling

and subsequent SEM imaging of the FIB x-sections were performed. A SEM image of a FIB-cross section of a 50 mN impact is shown in Figure 8 (a, b). It can be observed that there is no delamination between the coating and the substrate, showing that the bonding strength was high enough to sustain the impacting attack. In addition, it is clear that the plastic deformation is mainly in the substrate, and the coating thickness is almost uniform across the indented area. This result is consistent with the previous study that the dislocation-assisted plastic deformation was rather small in the coatings[36]. Furthermore, pronounced intercolumnar cracks through the whole thickness of CrN coating at the periphery of the indentation zone, and the transgranular cracks at the base of the coatings can be clearly observed in the cross-sectional morphology of impact craters (Fig. 8b).

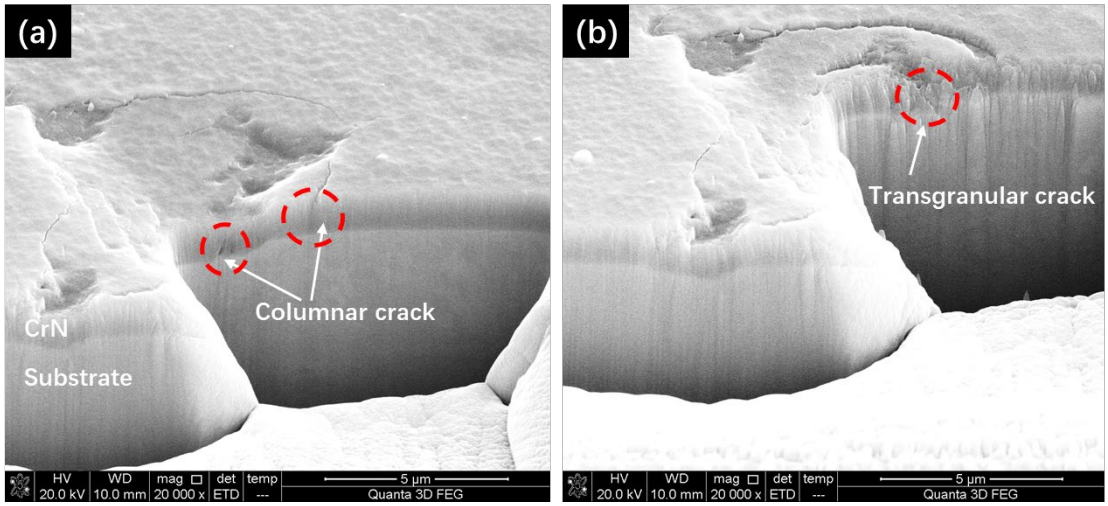

Fig. 8. (a) and (b) SEM cross-section images of different cracks under 50 mN impact loading.

The deformation of columnar films is dominated by the shear sliding of the coatings into the substrate at the onset of plastic deformation of substrate above a critical load[37]. However, the coating is generally not able to accommodate the resulting deformation of the underlying substrate due to the differences in elasto-plastic behavior close to the coating-substrate interface, which cause the development of tensile stresses parallel to the substrate surface within the coating, resulting in the generation of

intercolumnar cracks[36]. When the contact pressure is well above the plastic yielding onset of the substrate, the tensile radial stresses and strains existing in the vicinity of the residual imprint became large enough for inducing circumferential cracks at the coating surface[36.38]. In addition to the intercolumnar cracks in the cross-sectional examination of the impact impression at 50mN of acceleration force, lateral cracking is also visible at the base of the coating thickness reflected by the crack deflection, which may be responsible for the cohesive failure (spalling) occurring at the corner of the impact craters (Fig. 7). The impact deformation mechanism described above is similar to that observed in previous studies of indentation on columnar-like films[36.37.39-41]. In these stuides, the deformation behavior is considered as a composite response of a brittle film that undergoes shear sliding of the columnar grains and an underlying plastic flow in the ductile substrate at a critical stress, with the relatively weak columnar grain boundaries allowing the different types of cracks to occur within the coatings with increasing stress.

3.3.3. Fracture toughness analysis for CrN coating

In the past decade, significant progress has been achieved in evaluating the fracture toughness of hard coatings and thin films based on the stress and energy methods[42]. Nanoindentation is a most commonly used energy based method to produce a quantitative estimate of the fracture toughness by generating circumferential cracking and spallation of a brittle coating. Based on the 'step' in the load-displacement curve causing by a sudden excursion of the indenter, a formula to evaluate the fracture toughness (K_{Ic}) of hard coatings was suggested by Li *et al.*[43]:

$$K_{Ic} = \left[\frac{U_{fra} \cdot E}{(1-\nu^2) \cdot S}\right]^{1/2}, \qquad (2)$$

U_{fra} is the coating fracture energy, E and ν are Youngs modulus and Poissons ratio of the coating, respectively. S is the crack area and equals to $2\pi C_R t$ where C_R and t are the radius of circumferential through-thickness crack formed around the indenter, and the coating thickness, respectively. In this research, the thickness of the CrN coating is

about 2 μm and the length of the crack has been determined by open-source analysis software from the morphology of the residual impression. As can be seen from Fig. 7f, a well-developed circumferential cracking was generated on the surface of CrN coatings at 50mN acceleration load, and the parameters are summarized in Table 1.

Table 1. The data of C_R, S, v and E for CrN coating at 50mN.

Acceleration force (mN)	C_R **(um)**	S **(um²)**	v	E **(GPa)**
50	6.89	86.62	0.2	315

Based upon the analysis of first impact contact cycle, the total impacting energy (W_t) can be divided into four parts as[44]:

$$W_t = W_e + W_p + U_{fra} + W_o \quad (3)$$

where W_e is elastic storage work, W_p is the work of plastic deformation, U_{fra} is the fracture dissipated energy and W_o represents other energy loss such as the dissipated heat and friction work. The W_t and W_e can be measured by the kinetic energy at the contact $1/2mv_0^2$ and detachment $1/2mv_2^2$, respectively. Thus, the fracture energy U_{fra} can be simplified as

$$U_{fra} = {}^1/_2\, mv_0^2 - {}^1/_2\, mv_1^2 - W_p - W_0 \quad (4)$$

Clearly the determination of U_{fra} depends on the evaluation of the irreversible work of W_p and W_0. The W_0 can be approximated as the energy loss for the uncoated HSS substrate by omitting the W_f using Equation (5).

$$W_0 = W_t - W_p - W_e \quad (5)$$

Chen and Bull [45-47] proposed that the influence of cracking for a coated system can be averaged over the whole loading curve as the E/H remains almost constant and the ring-like cracking occurs during loading. Despites the presence of crack, the total indentation work will not be strongly affected because fracture only plays a role in

converting some stored elastic energy into irreversible work. In light of this, the W_p can be roughly estimated by Equation (6).

$$\frac{W_p}{W_t} = 1 - \gamma \frac{H}{E_r} \quad (6)$$

where E_r is the reduced indentation modulus and γ is an indenter geometry dependent constant. Typical value for γ is ~7 for metals and ~5 for glasses, with hard nanocomposite coating being commonly 5.7-6.4[8.48.49]. Chen *et al* [46] found that the calculated toughness for ZnO, SnO_2 and ITO coatings using such energy approach are similar to those by other method.

The relationship between energy ratio and H/E_r for the nano-impact has been previously verified by Constantinides *et al* [24] in quantitative single nano-impact testing with a Berkovich indenter on aluminum. Moreover, the plastic deformation for the CrN/HSS sample under large impact load was dominated by the substrate and the coated system can be treated as equivalent to a bulk material. When the indentation depth is greater than 800nm, the dimensionless parameter H/E_r remains almost constant, about 0.023 and 0.035 for the HSS and CrN/HSS, respectively (Fig. 2d).

Table 2. The calculated fracture dissipated energy and fracture toughness for CrN coating.

Sample	W_t **(nJ)**	W_e **(nJ)**	γ	W_p **(nJ)**	W_0 **(nJ)**	W_f **(nJ)**	K_{Ic} **(MPa•m1/2)**
HSS	484±5.0	24±0.7	7	407±4.8	54±0.6	/	/
CrN	543±4.8	51±2.3	5.7 ~6.4	422±3.6 ~435±3.8	54±0.6	2±0.5 ~16±0.7	2.75±0.3 ~7.74±0.5

Combined with Equation (2-6), the fracture dissipated work and the fracture toughness of the coating can be approximately estimated. The detailed data for the calculated energy at acceleration force of 50 mN was concluded in Table 2. To avoid the influence of indenter shape, the indenter geometry constant γ for CrN/HSS sample was taken as

5.7-6.4 in the calculation process, and the value of K_{Ic} was estimated in the range of 2.75-7.74 MPa•m$^{1/2}$, which is comparable with the reported data (K_{Ic} =3.13 MPa•m$^{1/2}$) of MS-PVD CrN coating determined by single-cantilever bending and pillar splitting experiments[50].

In summary, we provide a new insight to evaluate the dynamic fracture toughness of hard coatings based on the energy method by using nano-impact testing. However, the accurate extraction of irreversible work W_p during the impact process is still a great challenge, which is also the focal point of much debate in indentation fracture method. Besides, there are also some errors in the calculation of other dissipated energy W_0 due to the different impact depth of CrN/HSS and uncoated HSS substrate at the same acceleration load. Thus, further investigation will be done on the acquisition of indenter geometry constant γ and irreversible plastic work W_p during nano-impact for more precise quantification of the dynamic fracture toughness.

4. Conclusion

In this paper, the CrN coating was systematically investigated using the highly-resolved nano-impact over a wide range of acceleration load from 10mN to 50mN. It has been found the entire impact process can be divided into four stages as acceleration, indentation, rebound and deceleration stages, and there is a short “plateau” period in the 1st contact cycle of the CrN/HSS depth-time curves under high acceleration loads, which indicates the fracture of the coating. The FIB-SEM images evidenced the generation of intercolumnar cracks caused by the development of tensile stresses parallel to the substrate under impact loads. Based on the calculation formula of indentation fracture toughness and analysis of fracture energy dissipation, the dynamic fracture toughness was estimated in the range of 2.75-7.74 MPa•m$^{1/2}$ depending on the indenter geometry constant γ, which is comparable with the reported value of 3.13 MPa•m$^{1/2}$ in previous study. This work provides a new insight to evaluate the fracture toughness of hard coatings based on the nano-impact method.

5. Acknowledgments

The authors gratefully acknowledge the financial support from the NSFC (#11472080),

the NSF of Jiangsu Province (#BK20141336), the Fundamental Research Funds for the Central Universities, the financial support from the program of China Scholarships Council (No. 201706090126), and the postgraduate training innovation project of Jiangsu Province (KYLX16_0198).

References:

[1] C. Gautier, H. Moussaoui, F. Elstner, J. Machet, Comparative study of mechanical and structural properties of CrN films deposited by dc magnetron sputtering and vacuum arc evaporation, Surface and Coatings Technology, 86(1996) 254-262.

[2] S.Y. Lee, G.S. Kim, J.H. Hahn, Effect of the Cr content on the mechanical properties of nanostructured TiN/CrN coatings, Surface and Coatings Technology, 177-178(2004) 426-433.

[3] J.L. Mo, M.H. Zhu, A. Leyland, A. Matthews, Impact wear and abrasion resistance of CrN, AlCrN and AlTiN PVD coatings, Surface and Coatings Technology, 215(2013) 170-177.

[4] S. Krishnamurthy, I. Reimanis, Multiple cracking in CrN and Cr2N films on brass, Surface and Coatings Technology, 192(2005) 291-298.

[5] K.D. Bouzakis, G. Skordaris, S. Gerardis, E. Bouzakis, Nano-impact test on PVD-coatings with graded mechanical properties for assessing their brittleness, Materialwiss Werkst, 44(2013) 684-690.

[6] J. Chen, B.D. Beake, R.G. Wellman, J.R. Nicholls, H. Dong, An investigation into the correlation between nano-impact resistance and erosion performance of EB-PVD thermal barrier coatings on thermal ageing, Surface and Coatings Technology, 206(2012) 4992-4998.

[7] J. Chen, R. Ji, R.H.U. Khan, X. Li, B.D. Beake, H. Dong, Effects of mechanical properties and layer structure on the cyclic dynamic loading of TiN-based coatings, Surface and Coatings Technology, 206(2011) 522-529.

[8] J. Chen, H. Li, B.D. Beake, Load sensitivity in repetitive nano-impact testing of TiN and AlTiN coatings, Surface and Coatings Technology, 308(2016) 289-297.

[9] B.D. Beake, S.P. Lau, J.F. Smith, Evaluating the fracture properties and fatigue wear of tetrahedral amorphous carbon films on silicon by nano-impact testing, Surface and Coatings Technology, 177-178(2004) 611-615.

[10] B.D. Beake, Evaluation of the fracture resistance of DLC coatings on tool steel under dynamic loading, Surface and Coatings Technology, 198(2005) 90-93.

[11] N. Ravi, R. Markandeya, S.V. Joshi, V. Högskolan, F.I. Institutionen, F.A.O.A. Avdelningen, Fracture behaviour of nc-TiAlN/a-Si3N4 nanocomposite coating during nano-impact test, Surface Engineering, 33(2017) 282-291.

[12] B.D. Beake, S.R. Goodes, J.F. Smith, R. Madani, C.A. Rego, R.I. Cherry, T. Wagner, Investigating the fracture resistance and adhesion of DLC films with micro-impact testing, Diamond & Related Materials, 11(2002) 1606-1609.

[13] E. Frutos, J.L. González-Carrasco, T. Polcar, Repetitive nano-impact tests as a new tool to measure fracture toughness in brittle materials, Journal of the European Ceramic Society, 36(2016) 3235-3243.

[14] A.A. Voevodin, R. Bantle, A. Matthews, Dynamic impact-wear of TiC_xN_y and Ti-DLC composite

coating, Wear, 185(1995) 151-157.
[15] G.S. Fox-Rabinovich, B.D. Beake, J.L. Endrino, S.C. Veldhuis, R. Parkinson, L.S. Shuster, M.S. Migranov, Effect of mechanical properties measured at room and elevated temperatures on the wear resistance of cutting tools with TiAlN and AlCrN coatings, Surface and Coatings Technology, 200(2006) 5738-5742.
[16] N.H. Faisal, R. Ahmed, S. Goel, Y.Q. Fu, Influence of test methodology and probe geometry on nanoscale fatigue failure of diamond-like carbon film, Surface and Coatings Technology, 242(2014) 42-53.
[17] N.M. Jennett, J. Nunn, High resolution measurement of dynamic (nano) indentation impact energy: a step towards the determination of indentation fracture resistance, Philosophical Magazine, 91(2011) 1200-1220.
[18] B.D. Beake, J.F. Smith, Nano-impact testing—an effective tool for assessing the resistance of advanced wear-resistant coatings to fatigue failure and delamination, Surface and Coatings Technology, 188-189(2004) 594-598.
[19] B.D. Beake, S.R. Goodes, J.F. Smith, Micro-impact testing: A new technique for investigating thin film toughness, adhesion, erosive wear resistance, and dynamic hardness, Surface Engineering, 17(2001) 187-192.
[20] J.M. Wheeler, A.G. Gunner, Analysis of failure modes under nano-impact fatigue of coatings via high-speed sampling, Surface and Coatings Technology, 232(2013) 264-268.
[21] G.R. ANSTIS, P. CHANTIKUL, B.R. LAWN, D.B. MARSHALL, A Critical Evaluation of Indentation Techniques for Measuring Fracture Toughness: I, Direct Crack Measurements, Journal of the American Ceramic Society, 64(1981) 533-538.
[22] E.W. Andrews, A.E. Giannakopoulos, E. Plisson, S. Suresh, Analysis of the impact of a sharp indenter, International journal of Solids and Structures, 39(2002) 281-295.
[23] A. Ghosh, S. Jin, J. Arreguin-Zavala, M. Brochu, Characterization and investigation of size effect in nano-impact indentations performed using cube-corner indenter tip, Journal of Materials Research, 32(2017) 2241-2248.
[24] G. Constantinides, C.A. Tweedie, N. Savva, J.F. Smith, K.J. Van Vliet, Quantitative Impact Testing of Energy Dissipation at Surfaces, Experimental Mechanics, 49(2009) 511-522.
[25] A.C. Fischer-Cripps, Nanoindentation Test Standards, Springer New York, 2011.
[26] W.C. Oliver, G.M. Pharr, An improved technique for determining hardness and elastic modulus using load and displacement sensing indentation experiments, J. MATER. RES., 7(1992) 1564-1583.
[27] A. Matthews, A.R. Lefkow, Problems in the physical vapor-deposition of titanium nitride, Thin Solid Films, 126(1985) 283-291.
[28] C.N. Tai, E.S. Koh, K. Akari, Macroparticles on tin films prepared by the arc ion plating process, Surface and Coatings Technology, 43-4(1990) 324-335.
[29] A.C. Fischer-Cripps, Critical review of analysis and interpretation of nanoindentation test data, Surface and Coatings Technology, 200(2006) 4153-4165.
[30] A. Leyland, A. Matthews, Design criteria for wear-resistant nanostructured and glassy-metal coatings, Surface and Coatings Technology, 177-178(2004) 317-324.
[31] A. Leyland, A. Matthews, On the significance of the H/ E ratio in wear control: a nanocomposite coating approach to optimised tribological behaviour, Wear, 246(2000) 1-11.
[32] Y.W. Bao, W. Wang, Y.C. Zhou, Investigation of the relationship between elastic modulus and

hardness based on depth-sensing indentation measurements, Acta Materialia, 52(2004) 5397-5404.
[33] J.M. Wheeler, J. Dean, T.W. Clyne, Nano-impact indentation for high strain rate testing: The influence of rebound impacts, Extreme Mechanics Letters, 26(2019) 35-39.
[34] J. Chen, X. Shi, B.D. Beake, X. Guo, Z. Wang, Y. Zhang, X. Zhang, S.R. Goodes, An investigation into the dynamic indentation response of metallic materials, Journal of Materials Science, 51(2016) 8310-8322.
[35] X. Shi, B.D. Beake, T.W. Liskiewicz, J. Chen, Z. Sun, Failure mechanism and protective role of ultrathin ta-C films on Si (100) during cyclic nano-impact, Surface and Coatings Technology, 364(2019) 32-42.
[36] J.J. Roa, E. Jiménez-Piqué, R. Martínez, G. Ramírez, J.M. Tarragó, R. Rodríguez, L. Llanes, Contact damage and fracture micromechanisms of multilayered TiN/CrN coatings at micro- and nano-length scales, Thin Solid Films, 571(2014) 308-315.
[37] V. Jayaram, S. Bhowmick, Z.H. Xie, S. Math, M. Hoffman, S.K. Biswas, Contact deformation of TiN coatings on metallic substrates, Materials Science and Engineering: A, 423(2006) 8-13.
[38] D.F. Diao, K. Kato, K. Hokkirigawa, Fracture mechanism of ceramic coating in indentation, Journal of Tribology-transactions of the Asme, 116(1994) 860-869.
[39] L.W. Ma, J.M. Cairney, M.J. Hoffman, P.R. Munroe, Effect of coating thickness on the deformation mechanisms in PVD TiN-coated steel, Surface and Coatings Technology, 204(2010) 1764-1773.
[40] L.W. Ma, J.M. Cairney, M. Hoffman, P.R. Munroe, Deformation mechanisms operating during nanoindentation of TiN coatings on steel substrates, Surface and Coatings Technology, 192(2005) 11-18.
[41] L.W. Ma, J.M. Cairney, D. McGrouther, M. Hoffman, P.R. Munroe, Three dimensional imaging of deformation modes in TiN-based thin film coatings, Thin Solid Films, 515(2007) 3190-3195.
[42] S. Zhang, X. Zhang, Toughness evaluation of hard coatings and thin films, Thin Solid Films, 520(2012) 2375-2389.
[43] X.D. Li, D.F. Diao, B. Bhushan, Fracture mechanisms of thin amorphous carbon films in nanoindentation, ACTA MATER., 45(1997) 4453-4461.
[44] J. Chen, X. Shi, B.D. Beake, X. Guo, Z. Wang, Y. Zhang, X. Zhang, S.R. Goodes, An investigation into the dynamic indentation response of metallic materials, Journal of Materials Science, 51(2016) 8310-8322.
[45] J. Chen, Indentation-based methods to assess fracture toughness for thin coatings, Journal of Physics D: Applied Physics, 45(2012) 203001.
[46] J. Chen, S.J. Bull, Indentation fracture and toughness assessment for thin optical coatings on glass, Journal of Physics D: Applied Physics, 40(2007) 5401-5417.
[47] J. Chen, S.J. Bull, Investigation of the relationship between work done during indentation and the hardness and Young's modulus obtained by indentation testing, International Journal of Materials Research, 99(2008) 852-857.
[48] B.D. Beake, G.S. Fox-Rabinovich, S.C. Veldhuis, S.R. Goodes, Coating optimisation for high speed machining with advanced nanomechanical test methods, Surface and Coatings Technology, 203(2009) 1919-1925.
[49] Y. Choi, H. Lee, D. Kwon, Analysis of sharp-tip-indentation load–depth curve for contact area determination taking into account pile-up and sink-in effects, J. MATER. RES., 19(2004) 3307-3315.
[50] M. Sebastiani, K.E. Johanns, E.G. Herbert, G.M. Pharr, Measurement of fracture toughness by

nanoindentation methods: Recent advances and future challenges, Current Opinion in Solid State and Materials Science, 19(2015) 324-333.